Received: 5 May 2020 | Revised: 18 September 2020 | Accepted: 20 September 2020

DOI: 10.1111/ejss.13053

ORIGINAL ARTICLE

European Journal of Soil Science WILEY

Slippery liquid-infused porous surfaces: The effect of oil on the water repellence of hydrophobic and superhydrophobic soils

Rebecca McCerery[1] | **John Woodward**[1] | **Glen McHale**[2,3] | **Kate Winter**[1] | **Steven Armstrong**[2,3] | **Bethany V. Orme**[2]

[1]Department of Geography and Environmental Sciences, Faculty of Engineering and Environment, Northumbria University, Newcastle-Upon-Tyne, UK

[2]Smart Materials and Surfaces Laboratory, Faculty of Engineering and Environment, Northumbria University, Newcastle-Upon-Tyne, UK

[3]Institute for Multiscale Thermofluids, School of Engineering, University of Edinburgh, Edinburgh, UK

Correspondence
Rebecca McCerery, Department of Geography and Environmental Sciences, Faculty of Engineering and Environment, Northumbria University, Newcastle-upon-Tyne, NE1 8ST, UK.
Email: rebecca.mccerery@northumbria.ac.uk

Abstract

Soil wettability is important for understanding a wide range of earth system processes, from agricultural productivity to debris flows and sediment fan formation. However, there is limited research considering how soil–water interactions, where the soil grains are naturally hydrophobic, might change in the presence of oil from natural hydrocarbon leakage or oil spills. Here we show how slippery liquid-infused porous surfaces (SLIPS) apply to hydrophobic soils, by physical modelling of surfaces of different grain sizes and examining their interactions with water before and after impregnation with silicone oil. Using contact and sliding angle measurements and laser scanning fluorescence confocal microscopy, we demonstrate that soil SLIPS can be created with thick oil layers and thin conformal oil layers on median grain sizes of 231 μm and 32 μm, respectively. Until now, SLIPS have only been observed in human-made materials and biological surfaces. The mechanisms reported here demonstrate that SLIPS can occur in natural granular materials, providing a new mechanism for water-shedding in soil and sediment systems. Furthermore, the water-shedding properties may be long lasting as conformal oil layers are stabilized by capillary forces. These results have important implications for understanding soil physics and mechanics where oil is present in a soil, and for agricultural hydrophobicity on shallow slopes.

Highlights

- We model oil contamination on a hydrophobic model soil as a mechanism for creating SLIPS.
- Soil SLIPS have implications for water-shedding, oil spill remediation and earth processes.
- Our model soils exhibit extreme water-shedding, illustrated by low water droplet sliding angles.

- This is the first physical modelling observation of SLIPS arising from hydrophobic soil.

KEYWORDS

earth processes, hydrophobicity, oil contamination, sediments, slippery liquid-infused porous surfaces, soil systems, soil water repellence, superhydrophobicity

1 | INTRODUCTION

Wettability is a measure of a soil's affinity for water. Water-repellent, or hydrophobic, soil has a low affinity for water and low rates of infiltration, with hydrological and geomorphological consequences (Jordán, Zavala, Mataix-Solera, & Doerr, 2013). Water-repellent soils are prevalent across the world in different climates and environments, from the sub-tropics to the Arctic (Dekker & Ritsema, 1994; Jordán et al., 2013). The negative consequences of water repellence are widely reported; one of the most observed is a reduction in soil productivity. This is widespread in southern and western Australia, which contains the world's largest area of water-repellent soils, with over 5 million hectares of agricultural land being affected (Blackwell, 2000). Water repellence leads to poor agricultural productivity due to the formation of preferential flow paths and finger flow, which affects the transport of water and solutes (Shakesby, Doerr, & Walsh, 2000; van Ommen, Dekker, Dijksma, Hulshof, & van der Molen, 1988; Wang et al., 2018). In some circumstances, this can also lead to groundwater contamination through leaching of pesticides and other substances (Blackwell, 2000; Van Dam et al., 1990). Water repellence also influences surface processes as soils become more susceptible to both water and wind erosion (Cannon, Bigio, & Mine, 2001; Cannon, Gartner, Wilson, Bowers, & Laber, 2008; Parise & Cannon, 2012). High water repellence can increase the occurrence of debris flow events, considered to be one of the most destructive consequences of soil water repellence with a known risk to human life (DiBiase & Lamb, 2020). However, a reduction in water infiltration can also have beneficial consequences, by improving the structural and aggregate stability of affected soils (Bachmann et al., 2008; Hallett, Baumgartl, & Young, 2001). For hydrophobic soil, this stability can also lead to reduced evaporation of water from deep within the soil profile (Hallett, 2007); a similar process also increases carbon sequestration, through reduced biodegradation of organic matter or increased aggregate stability (Bachmann et al., 2008; Piccolo, Spaccini, Haberhauer, & Gerzabek, 1999; Spaccini, Piccolo, Conte, Haberhauer, & Gerzabek, 2002).

There are at least five pathways by which water repellence can be induced in soil environments. First, it can be created beneath particular types of plants (DeBano, 2000; Doerr et al., 2006; Doerr, Ritsema, Dekker, Scott, & Carter, 2007; Doerr, Shakesby, & Walsh, 2000). This occurs where hydrophobic waxes and other organic substances create a coating on the soil grains through degradation of plant litter (Doerr, Shakesby, & Walsh, 1996). This is common in eucalyptus forests, where water repellence can develop rapidly after eucalyptus is planted on previously hydrophilic soil (Doerr, Shakesby, & Walsh, 1998). Second, the presence of hydrophobins (small amino acids found in filamentous fungi such as mycelia) (Wessels, 1996) can induce water repellence due to the inherent hydrophobicity of the hydrophobin proteins on the fungi surface (Chau, Goh, Vujanovic, & Si, 2012; Linder, 2009). A similar process caused by bacteria extracellular polymeric substances has also been linked to soil water repellence, with the creation of hydrophobic bacterial biofilms by certain species (Doerr et al., 2007; Schaumann et al., 2007). Third, wildfire events burning organic materials can cause volatilization of waxes in the surface litter, creating a hydrophobic coating on affected soil grains (DeBano, 2000; Doerr et al., 2000, 2006; McHale, Shirtcliffe, Newton, Pyatt, & Doerr, 2007). This process is commonly seen in the western USA and can result in increased runoff and erosion (Woods, Birkas, & Ahl, 2007). The fourth mechanism is the disposal of wastewater into the environment. This occurs through irrigation of soils using greywater, containing oil, grease and other hydrophobic compounds, a practice that is increasing in regions of the world that experience water scarcity (Hamlett et al., 2011; Maimon, Gross, & Arye, 2017; Mataix-Solera et al., 2011). Finally, oil contamination either through direct oil spills or hydrocarbon seepage from sedimentary basins can induce water repellence (Ellis & Adams, 1961; McHale, Shirtcliffe, Newton, Pyatt, & Doerr, 2007; Roy & McGill, 1998). Oil contamination is particularly difficult to remediate, with water repellence persisting for decades after contamination (Roy, McGill, & Rawluk, 1999). For example, crude oil spill sites in Alberta, Canada, have been unable to naturally rectify themselves after oil spills in Devon in 1947 and Bruderheim in 1982 (Roy & McGill, 1998). These soils continue to be non-wettable and unable to support plant growth (Roy et al., 1999; Roy & McGill, 1998, 2000).

Several structural and environmental properties influence the expression of water repellence in soils. Smaller, sand-sized grains tend to display the highest degree of water repellence, attributed to the existence of gaps between grains and a higher organic matter content (de Jonge, Jacobsen, & Moldrup, 1999; Doerr et al., 1996, 2007; McHale, Shirtcliffe, Newton, & Pyatt, 2007). Studies have also attempted to correlate changes in soil water content (e.g. de Jonge, Moldrup, & Jacobsen, 2007; Dekker, Doerr, Oostindie, Ziogas, & Ritsema, 2001; Leelamanie & Karube, 2007; Regalado & Ritter, 2006) and soil temperature (e.g., de Jonge et al., 1999; Doerr et al., 2007; Doerr, Dekker, Ritsema, Shakesby, & Bryant, 2002; Jordán et al., 2013; van Ommen et al., 1988) with different degrees of hydrophobicity, but contradictory results suggest these processes are not fully understood.

2 | CONCEPTS OF WATER REPELLENCE

Soil water repellence can be measured in the field and the laboratory using a range of water-droplet methods. When a droplet rests on a surface, it will adopt a shape based on its volume and liquid surface tension (γ_{LV}), and the surface properties, influenced by the extent of their water repellence. For small droplets, of a size less than the capillary length (l_c):

$$l_c = (\gamma_{LV}/\rho g)^{1/2}, \quad (1)$$

where ρ is the liquid density and $g = 9.81\ \mathrm{ms}^{-2}$ is the acceleration due to gravity; capillary forces dominate over gravity, creating a spherical cap shape. When the surface is granular, like soils, evaporation and infiltration of water into the pore structure may occur over time, with their relative importance determined by the wettability (Letey, Osborn, & Pelishek, 1962). If infiltration is more prevalent than evaporation, water drop penetration time (WDPT) measurements can be employed (Robichaud, Lewis, & Ashmun, 2008; Tessler, Wittenberg, Malkinson, & Greenbaum, 2008). If droplets do not infiltrate rapidly, a contact angle (θ) may be measured from the side profile of a droplet. This method was adapted by Bachmann, Ellies, and Hartge (2000) for use in characterizing the wettability of soils, whereby monolayers of soil particles were fixed to a surface to capture the wetting properties through contact angle measurements on the interfacial layer.

For an ideal simple solid with a flat surface, the interfacial tensions, γ_{IJ}, of the solid–liquid, solid–vapour and liquid–vapour interfaces determine the ideal contact angle, θ_e, described by Young's Law (Equation (2)) (Figure 1a) (Young, 1832):

$$\cos\theta_e = \frac{\gamma_{SV} - \gamma_{SL}}{\gamma_{LV}}. \quad (2)$$

The hydrophobic coatings on soil grains have different surface energies than the grains without a hydrophobic coating, influencing the action of the three-phase contact line shown in Figure 1. Grains with a lower surface energy coating than water will lead to a degree of water repellence (Roy & McGill, 2002). Young's Law, however, is only applicable to ideal solid flat surfaces (Leelamanie & Karube, 2012). Where the surface is rough, structured or granular/porous, such as that created by soil grains, a droplet will interact with (or wet) the structure in several different ways. The droplet may sit in a pure Cassie-Baxter state (Cassie & Baxter, 1944), suspended on the tops of the solid protrusions, bridging air pockets that are unfavourable for water penetration

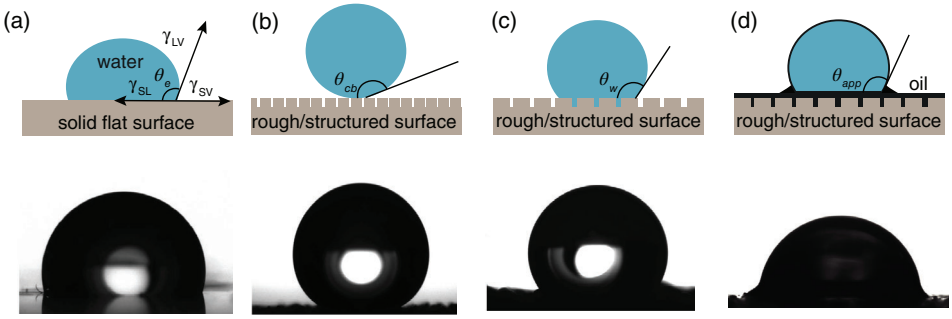

FIGURE 1 Four models of water interaction with different surfaces and corresponding droplet images (10 μL). Panels (a) to (d) show: a water droplet on (a) a smooth flat surface with contact angle (θ_e) controlled by the solid–liquid (γ_{SL}), solid-vapor (γ_{SV}) and liquid–vapor (γ_{LV}) interfaces; (b) a rough/structured surface with air in the gaps representing a Cassie-Baxter state and contact angle (θ_{cb}); (c) a rough/structured surface with water penetration representing a Wenzel state and contact angle (θ_w); and (d) a slippery liquid-infused porous surface (SLIPS) state and apparent contact angle (θ_{app}). The surface roughness/structure in the lower panels of (b) to (d) is caused by the granular nature of the hydrophobic surface [Color figure can be viewed at wileyonlinelibrary.com]

because of the interfacial forces (Figure 1b). In this case, the contact angle increases beyond that created by the surface chemistry alone. The decreased contact of the droplet with the solid makes the droplet highly mobile, and this is known as a "slippy" surface (Bachmann et al., 2006; Cassie & Baxter, 1944; Quére, Lafuma, & Bico, 2003). Where the droplet fully penetrates the surface structure, maintaining complete contact of water with the solid, a Wenzel state is entered (Wenzel, 1936). This results in a pinned and immobile droplet, and the solid is deemed a "sticky" surface (Figure 1c) (Dai, Stogin, Yang, & Wong, 2015; Quére et al., 2003; Wenzel, 1936). These effects can occur on biological surfaces (i.e., sacred lotus leaves) (Barthlott & Neinhuis, 1997; Neinhuis, 1997) and can be synthetically created through chemical alterations and the creation of micro- and nanostructures (Roach, Shirtcliffe, & Newton, 2008). They have also been observed in granular materials such as soils and sediments, where studies have shown that changing grain size has some influence over the degree of water repellence, with smaller grains displaying more water repellence (Bachmann, Horton, van der Ploeg, & Woche, 2000; de Jonge et al., 1999). Surfaces that are observed to have extremely high static contact angles (above 150°) (Erbil, Demirel, Avci, & Mert, 2003), where static refers to the contact angle observed in a side profile directly after droplet deposition, and which move easily at low angles of surface tilt are referred to here as superhydrophobic. In these concepts, a key assumption for a surface formed by grains is that the droplet does not lift the grains and coat itself due to capillary forces (i.e., a liquid marble effect does not occur) (Aussillous & Quéré, 2001).

As shown by the Wenzel state (Figure 1c), a high contact angle surface is not necessarily a slippery surface with good water-shedding properties, where water-shedding refers to the ease with which a droplet moves on a surface (via rolling or slipping) with minimal force (Quére et al., 2003). Excellent water-shedding abilities can be achieved through low contact angle hysteresis irrespective of the absolute value of the static contact angle (see Tao et al., 2020) and is typically seen when a droplet interacts with a surface in a Cassie-Baxter state where there is less solid–liquid contact (McHale, Newton, & Shirtcliffe, 2005). However, water-shedding surfaces can also be created by exposing structured, rough or granular/porous hydrophobic surfaces to oil, to create bio-inspired slippery liquid-infusedporous surfaces (Wong et al., 2011) and lubricant-impregnated surfaces (LIS) (Lafuma & Quéré, 2011; Smith et al., 2013). SLIPS/LIS technology aims to replicate the excellent slippery surfaces of the *Nepenthes* pitcher plant by taking inspiration from its nanostructures, lubricative surface chemistry and hygroscopic nectar and applying it to synthetic materials, for purposes such as anti-biofouling and ice repellence (Bauer & Federle, 2009; Nosonovsky, 2011; Wang, Zhang, & Lu, 2015; Wilson et al., 2013). In SLIPS an infused oil preferentially (compared to water) and completely wets the solid due to its surface chemistry, thus providing a continuous oil surface on which the water droplet rests (McHale, Orme, Wells, & Ledesma-Aguilar, 2019; Wong et al., 2011). It remains possible to observe an (apparent) static contact angle, θ_{app}, which for vanishingly thin layers of oil can be predicted from a liquid form of Young's law, but the value of which decreases as the thickness of the oil increases (McHale et al., 2019; Semprebon, Mchale, & Kusumaatmaja, 2017). Because the water only ever contacts the immiscible oil (and not the solid), there is a lubricating effect reducing surface friction, creating excellent water-shedding abilities demonstrated by very small water droplet sliding angles, typically $\leq 5^{\circ}$ for a droplet ≥ 2 μL. (Figure 1d) (Wang et al., 2015; Wong et al., 2011). These sliding angles, and the observed contact angle hysteresis (albeit small), are then dependent on the thickness of the oil layer (Semprebon et al., 2017). A significant characteristic of these surfaces is their ability to lock-in and retain a thin oil layer (due to capillary forces from the surface chemistry), which cannot be displaced by water, resulting in stable and long-term water-shedding properties (Bauer & Federle, 2009; Nosonovsky, 2011; Wang et al., 2015; Wilson et al., 2013).

Until now, the creation of SLIPS has never been proposed for soils or demonstrated in model hydrophobic soils. We hypothesize that exposing hydrophobic soils to oil can cause them to acquire enhanced water-shedding properties without the need for the high contact angles required for a hydrophobic soil. This mechanism is analogous to that used by the *Nepenthes* pitcher plant to create a super-slippery surface, which has been mimicked in materials science with slippery liquid-infused porous surfaces (SLIPS). We aim to identify a mechanism by which soils and other granular materials such as sediments can form SLIPS and how this will affect their water repellence and water-shedding properties. We achieve this by replicating oil contamination on model hydrophobic soils and characterizing these surfaces using water droplet contact angles and sliding angles.

3 | EXPERIMENTAL METHODS

3.1 | Preparation of model soils

To create model soils we used monolayers of grains attached to a glass slide as outlined by the Bachmann, Ellies, and Hartge (2000) method for performing the

TABLE 1 Grain sizes used in this study, with the corresponding grain size classification of Wentworth and the spin speed used for polydimethylsiloxane (PDMS) coating, PDMS thickness for each grain size and the % void space for the final surface

Grain size range (μm)	Median grain size (μm)	Median phi size (ϕ)	Wentworth conversion	Spin speed (rpm) for 5 min	PDMS thickness (μm)	% void space
4–25	15	6.47	Clay aggregates	6,000	5	14
9–54	32	5.50	Medium silt	6,000	5	15
32–63	58	4.47	Coarse silt	6,000	5	19
63–90	77	3.73	Very fine sand	6,000	5	19
90–125	108	3.24	Very fine sand	5,000	6	17
125–180	153	2.74	Fine sand	5,000	6	21
180–212	196	2.35	Fine sand	5,000	6	14
212–250	231	2.12	Fine sand	5,000	6	16
250–300	275	1.87	Medium sand	4,000	7	17
300–355	328	1.61	Medium sand	4,000	7	27
355–712	533	0.99	Coarse sand	4,000	7	27

sessile drop method on soils. Silver-grade general purpose silica sand (sourced from Fisher Scientific, Loughborough, UK), silica silt (sourced from Fantasy Quartz Sand Supply, Kowloon, Hong Kong) and kaolin clay (sourced from American Elements, Los Angeles, California) were sieved into grain-size fractions (shown in Table 1). Sand, silt and clay of different grain sizes were used to recreate the natural roughness, shape and size of a soil surface as per Bachmann et al. (2000) and Bachmann, Goebel, and Woche (2013) for our model soils. This method was chosen over using glass spheres, another method of modelling hydrophobic soils. Previous works have used uniform glass spheres to model soils without any chemical or mechanical alterations to the surface; this tends to limit the contact angles of model soils as they remove the soil surface texture and high aspect ratio, which are critical in creating extreme water repellence (McHale, Shirtcliffe, Newton, & Pyatt, 2007; Shirtcliffe et al., 2004). To combat this, some studies have applied chemical or mechanical action to the uniform glass spheres, creating a degree of surface roughness (Ibekwe, Tanino, & Pokrajac, 2019; Utermann, Aurin, Benderoth, Fischer, & Schröter, 2011). However, for this study, we preferred to use a natural material with surface roughness more reflective of the natural environment, rather than an artificially created synthetic analogue.

Grains were cleaned as per Hamlett et al. (2013); they were first immersed in (3% v/v in water) HCl for 24 hr and rinsed with deionised water, then re-immersed in (3% v/v in water) HCl for 3 hr. The concentration of HCl was gradually increased to 30% and the grains left for 1 hr before being rinsed with deionised water, 5 M KOH solution, and again with deionised water at 1:1 grains:solution three times or until the solution ran clear. The grains were then re-immersed in (3% v/v in water) HCl for a further 16 hr before being rinsed with deionised water at a ratio of 1:2 grains:water a minimum of five times or until the solution ran clear, and dried at 100°C for 24 hr. The dried grains were hydrophobized by immersion in a bath of Grangers Footwear Repel (a non-pore-clogging siloxane-based hydrophobizing agent) as per Atherton et al. (2016), Hamlett et al. (2013) and McHale, Shirtcliffe, Newton, Pyatt, and Doerr (2007) for 24 hr and dried at 70°C for 6 hr. This ensured the surface chemistry of all types of grains was uniform, by creating a nanometric coating of the siloxane-based hydrophobizing agent on each grain (independent of mineralogy), and that our model soils satisfied two of the key conditions for SLIP surfaces: (a) the lubricating oil must wick into, wet and stably adhere within the substrate and (b) preferential wetting by oil compared to water. Thus, the oil forms a completely wetting film on the model soil when in air and, in the presence of a droplet of water, this wetting film of oil is maintained between the model soil and the droplet. To allow for tilting experiments and to prevent the creation of liquid marbles, the grains were fixed using a glass microscope slide coated with polydimethylsiloxane (PDMS) at a thickness of 5–7 μm, measured by a stylus profilometer (Bruker DektakXT) (Figure 2). The PDMS mixture (10:1 elastomer to curing agent ratio) was degassed for 45 min and then spun to the correct thickness for each grain size (Table 1) using a spin coater within 30 min of degassing at 5000–6000 rpm for 5 min. Loose sand grains were sprinkled onto the PDMS surface and agitated by hand for 10 s to prevent clumping of grains, then placed in the oven at 120 °C for 5 hr to cure. Excess sand was shaken off and the surface was rinsed with deionised water to prevent the formation of liquid marbles.

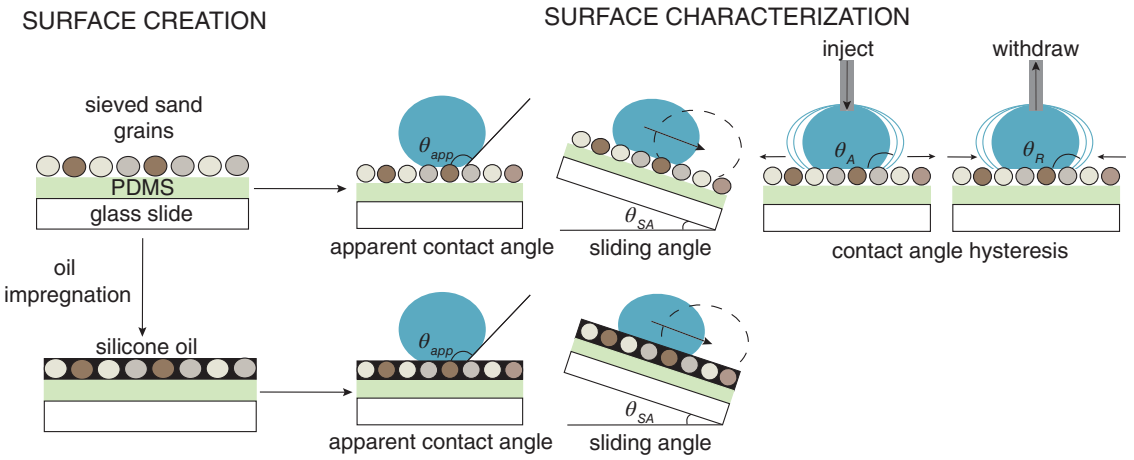

FIGURE 2 Schematic illustrating surface creation and characterization techniques. Surfaces were created using sieved sand, silt and clay grains that were hydrophobized using a commercial hydrophobizing agent and attached to a glass microscope slide using polydimethylsiloxane (PDMS). The hydrophobic oil-free surfaces were characterized by measuring the apparent contact angles (θ_{app}), sliding angles (θ_{SA}) and advancing (θ_A) and receding (θ_R) angles to determine the contact angle hysteresis. Surfaces were then impregnated with silicone oil using three different withdrawal speeds. Oil-impregnated samples were characterized by measuring the apparent contact angles (θ_{app}) and sliding angles (θ_{SA}) [Color figure can be viewed at wileyonlinelibrary.com]

The void fraction of the surface was measured by using microscope images of each surface and inputting these images into a MATLAB code. The code is designed to find the void fraction of the image by creating a binary image before calculating the ratio of particles versus pore space as the ratio of black to white space. The percentage void space for each of our surfaces is stated in Table 1.

3.2 | Oil impregnation

Oil contamination was replicated by impregnating all hydrophobic samples with 20cSt silicone oil (Figure 2), made fluorescent for detection with the laser scanning fluorescence confocal microscope (LSFCM) by dosing with a solution of Nile Red at a 0.01% by weight ratio. Three scenarios of oil impregnation were modelled to represent different environmental conditions. Thick oil layers were used to simulate environments where excess oil has contaminated soil and filled all the pore spaces between the individual grains. Thin oil layers were used to simulate an environment where oil still penetrates all of the spaces between the grains but leaves only a thin coating on the top of the surface. The thinnest oil layers simulate an environment where all excess oil has drained away, leaving a conformal oil layer across each grain, stabilized by capillary forces formed by the hydrophobic chemistry but with the limited filling of excess oil in the pore spaces. The dip coating was performed using a dip-coating machine (Fisnar F4200N) with adjustable and controlled withdrawal speeds, with an accuracy of ± 0.02 mm s^{-1}. The surfaces were fully immersed in the bath of silicone oil for 10 s before being vertically withdrawn at a set constant speed according to the desired oil thickness as per Geraldi et al. (2019). The silicone oil preferentially coated the grains due to the hydrophobic chemistry and by controlling the withdrawal speed of the surface from the oil bath it was possible to control the oil thickness, with a faster withdrawal speed producing a thicker layer of oil (Landau & Levich, 1988; Seiwert, Clanet, & Quéré, 2011). The thick oil layer was created by withdrawing the samples at 0.5 mm s^{-1}, the thin oil layer was created by withdrawing the sample at 0.1 mm s^{-1}, and the thinnest (or conformal) oil layer was created by withdrawing the samples at 0.1 mm s^{-1} and suspending them for 24 hr to remove excess oil, leaving only the thinnest possible thermodynamically stable oil layer. To measure the changes in oil thickness with increasing grain size as well as withdrawal speed, a Nikon A1 SHS laser scanning fluorescence confocal microscope was used to measure the oil thickness (thick, thin and thinnest) on the four surfaces we created, with median grain sizes of 15 μm (phi 6.47), 77 μm (phi 3.73), 231 μm (phi 2.12) and 533 μm (phi 0.99).

3.3 | Water droplet contact angle measurements

The apparent (static) water droplet contact angle, θ_{app}, was measured using a Krüss Droplet Shape Analyser (DSA30) at ambient room temperature (20–25°C). Using the sessile drop method, a 10 μL droplet of deionised water was placed on the horizontally mounted surface

and a side-view image of the two-dimensional profile of the droplet was taken (Figure 2). This was repeated 10 times per surface at different locations across the surface. The open source program PyDSA was used to analyse the images taken on the Krüss DSA30 to determine the θ_{app}. The PyDSA OpenCV Canny edge detection function was used to detect the edges of the droplet and a fixed straight baseline was used to measure the triple-phase point where the droplet makes contact with the surface (Launay, 2018). This multistage algorithm detected the edge between two threshold values while filtering noise to give a single smooth edge (Canny, 1986). This returned an array of coordinates showing where the edge was detected. The programme then performs an elliptical fit using the fitEllipse function in the OpenCV library, which uses the Fitzgibbon direct least square fitting method to obtain these values, taking the contact angle from the tangent of the fitted ellipse and the baseline (Fitzgibbon, Pilu, & Fisher, 1999; Launay, 2018).

3.4 | Water droplet contact angle hysteresis measurements

Contact angle hysteresis (CAH) was measured using the advancing (θ_A) and receding (θ_R) contact angles of water droplets, which shows the range of contact angles a droplet can take on a surface whilst the contact line remains stationary. A superhydrophobic surface will exhibit low hysteresis as the droplet easily de-pins from the surface. We measured the CAH on the hydrophobic surfaces before oil impregnation by increasing and decreasing the volume of water in the droplet until the contact line was observed to move (Figure 2). Measurements were recorded with the inbuilt video sequencing software on the Krüss DSA30 at five frames per second to capture the inflation and deflation of the water droplet. The advancing contact angle was measured by depositing a 6 μL droplet on the surface and adding 10 μL of water at 10 μL min^{-1} into the droplet. The droplet was left to stabilize for 10 s before the receding angle was measured by withdrawing 10 μL of water at 10 μL min^{-1}. This was repeated 10 times at different locations across the surface.

The videos were then analysed using Image J. The advancing and receding frames were extracted from the full video by importing the frames into ImageJ and stepping through the video one frame at a time. For the determination of the advancing frame, the "zoom tool" was used in ImageJ to focus on the contact point of the shadow graphed droplet. The frame at which the black pixel of the droplet advanced, or filled the white pixels of the background, was deemed to be the frame post θ_A. The frame prior is where θ_A was measured as the droplet will have assumed the largest angle possible on that surface before the inflation forced the droplet to grow in terms of droplet footprint. To measure θ_A the "angle tool" in ImageJ was used. The baseline was placed at the bottom of the droplet (on the sample) and the angle fitted as a tangent to the side of the droplet where the black pixels turn to white pixels near the contact point. The same process was followed for θ_R, where the receding frame was determined by the retraction of the contact line, or where the black pixels of the droplet turn into white background. The CAH for the surface can then be calculated using Equation (3):

$$\Delta\theta_{CAH} = \theta_A - \theta_R. \quad (3)$$

Due to the pinning of water droplets onto asperities of individual grains, some advancing and receding angles could not be measured (the number of data points excluded due to pinning for each grain size can be found in the Supporting Information). Furthermore, CAH on SLIPS, with their highly mobile contact line with minimal pinning points, are small (within contact angle measurement error) (Guan et al., 2015; Wong et al., 2011). For this reason, the SLIPS literature focuses on sliding angle measurements for a defined droplet volume to characterize droplet mobility.

3.5 | Water droplet sliding angle measurements

Water droplet sliding angles (θ_{SA}) were used to determine the water-shedding ability of the hydrophobized surfaces before and after impregnation with silicone oil using the Krüss DSA30 tilt table. The θ_{SA} was measured as the substrate angle (where the surface is tilted from the horizontal) at which the water droplet unpinned from its position and began to move on the inclined surface (Cui et al., 2019) (Figure 2). The platform was levelled using a spirit level before tilting each surface. A droplet of 20 μL was then deposited on the surface and slowly inclined at 0.2° per second until the droplet began to move. The sliding angle was measured on both the hydrophobic samples with no oil impregnation and each silicone oil impregnation scenario. Ten sliding angles were measured for each surface. The Krüss DSA30 proprietary software (DSA4) was used to determine the θ_{SA} within an error of ±0.2°.

4 | RESULTS

Figure 3a shows apparent, advancing and receding contact angles, and hence CAH, as a function of grain size.

The CAH is the difference between the advancing (triangle) and receding (diamond) contact angles and the independently measured apparent contact angle is shown as a dashed line in Figure 3a. The apparent contact angle of around 150° and a CAH of less than 10° shows that at median grain sizes of 15 μm (phi 6.47), droplets are clearly in a superhydrophobic state. The overall trend shows apparent decreasing of the contact angle and CAH increasing with increasing grain size.

Sliding angles were also measured for these surfaces before oil impregnation (shown in Figure 3b). Small sliding angles were observed at the lowest grain size, with sliding angles increasing as grain size increased. This trend shows that droplets at low grain sizes are highly mobile, which is consistent with the low CAH and high apparent contact angles at low grain sizes in Figure 3a. The inset images in Figure 3b show the maximum recorded angle before water droplets slide on our model hydrophobic soils. The low sliding angle at the smallest grain size and the retention of the droplet on the near-vertical surface at the highest grain size dramatically illustrate the concepts of "slippy" and "sticky" surfaces we introduced in the *Concepts of Water Repellence* section. Figure 3b also shows a plateau in sliding angle on median grain sizes 58-275 μm (phi 4.47–1.87), where the droplets are in neither a pure Cassie-Baxter nor a Wenzel state.

Figure 4a shows apparent contact angles of water on our model hydrophobic soils, after impregnation with oil and then allowing the oil to drain to the thinnest possible layer as a function of grain size. The inset images show droplets of water with similar contact angles of between 86° and 98° across the full range of grain sizes. These images can be contrasted with the clear decrease in apparent contact angle with increasing grain size (inset images in Figure 3a) for the model hydrophobic soils before oil impregnation.

Sliding angles were also measured for the oil-impregnated hydrophobic model soils, shown in Figure 4b. At the lowest median grain size of 15 μm (phi 6.47), the sliding angle of between 1° and 3° is lower than the superhydrophobic state for the model hydrophobic soil shown in Figure 3b. As the grain size increases the sliding angle also slowly increases, but it remains lower than the sliding angles in the intermediate state for the model hydrophobic soils (shown in Figure 3b). The inset droplet images in Figure 4b show the maximum sliding angle on the model hydrophobic soils with the thinnest oil layer. The contrast in the maximum sliding

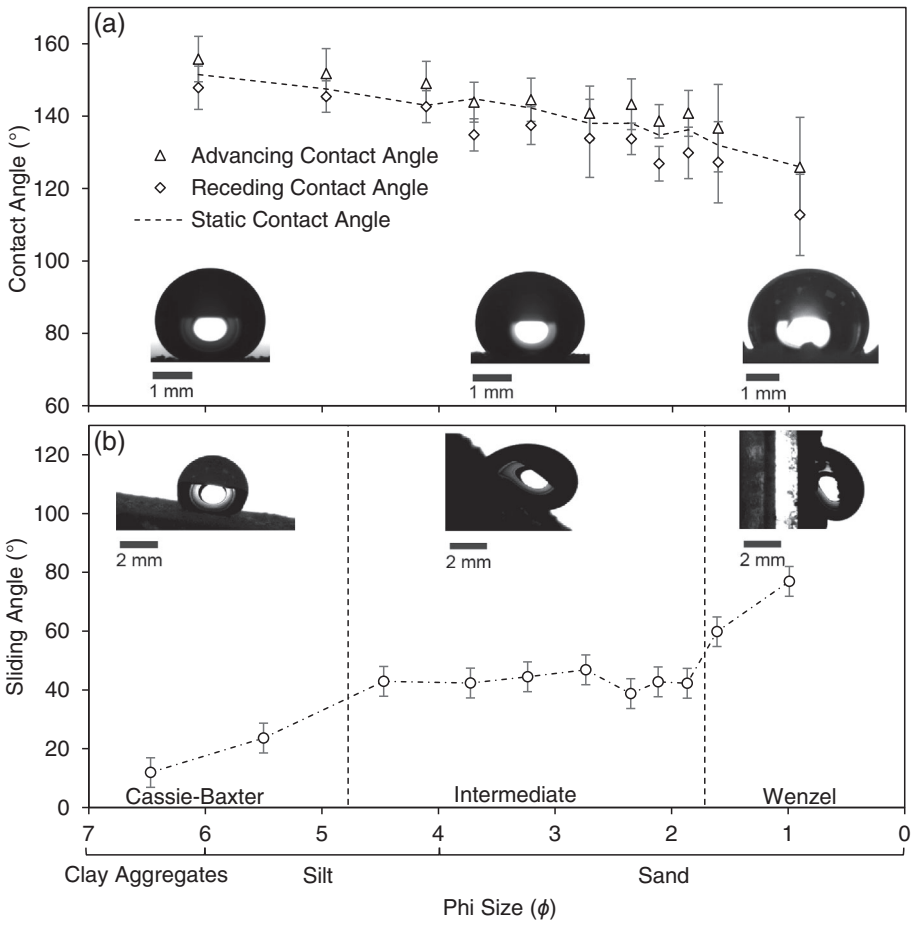

FIGURE 3 (a) Median advancing, receding and apparent contact angles on model hydrophobic soil (with standard deviation error bars, produced from 10 measurements per surface using a 10 μL droplet). The inset images are a droplet on (from left to right) clay aggregates, fine sand and coarse sand. (b) Median sliding angles on model hydrophobic soil without oil impregnation (with standard deviation error bars, produced from 10 measurements per surface using a 20 μL droplet). The inset images are a droplet on an inclined surface at the point of depinning on (from left to right) clay aggregates, fine sand and coarse sand

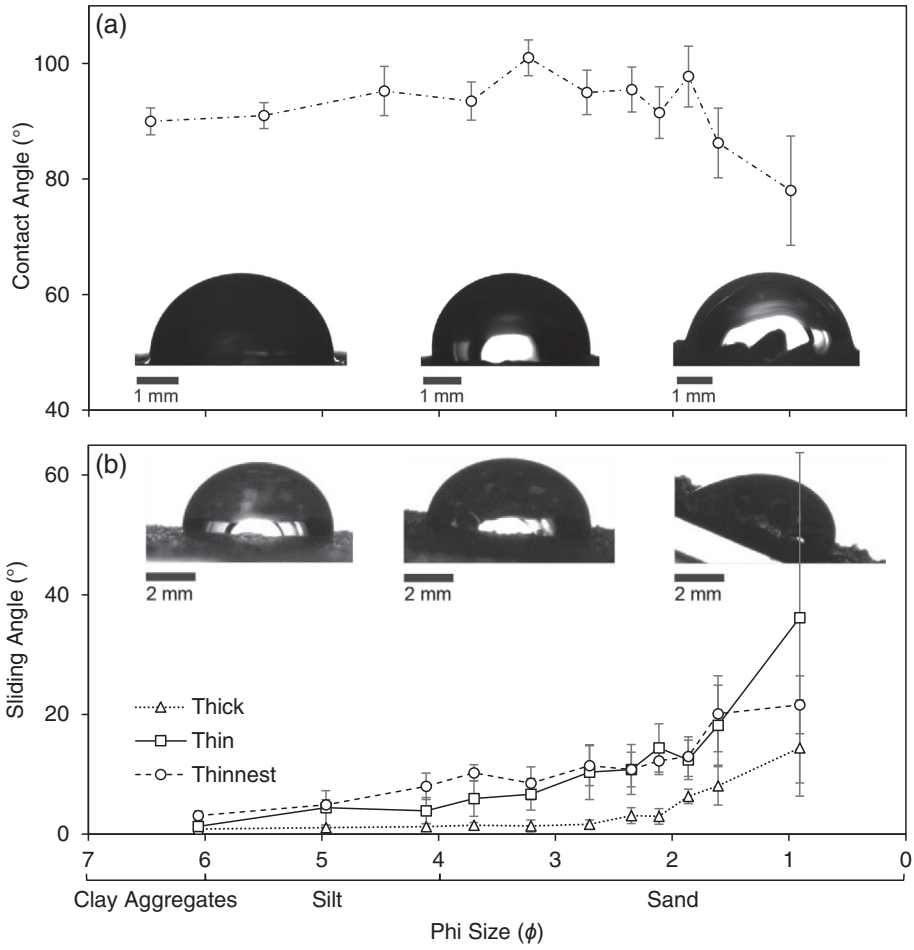

FIGURE 4 (a) Median apparent contact angles on the thinnest oil layer (with standard deviation error bars, produced from 10 measurements per surface using a 10 μL droplet). Inset images show a droplet on a conformal oil layer on (from left to right) clay aggregates, fine sand and coarse sand. (b) Median sliding angles of water droplets on oil impregnated surfaces (with standard deviation error bars, produced from 10 measurements per surface using 20 μL droplets). Inset images show a droplet on a conformal oil layer at the point of depinning on (from left to right) clay aggregates, fine sand and coarse sand

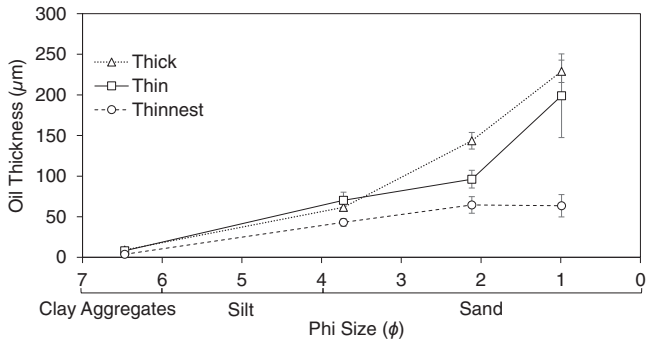

FIGURE 5 Oil thickness measurements taken on the laser scanning fluorescence confocal microscope for the thinnest, thin and thickest oil layer scenarios, for median grain sizes 15 μm (phi 6.47), 77 μm (phi 3.73), 231 μm (phi 2.12) and 533 μm (phi 0.99)

angle between the inset images in Figures 3b and 4b illustrates the significant increase in water-shedding ability of the oil-impregnated hydrophobic model soils, particularly at the higher grain sizes. The trends in Figure 4b are the same regardless of whether we consider the thinnest coating of oil or the thicker layers of oil. The water-shedding ability of oil-impregnated hydrophobic model soils remains strong even with the thinnest coating of oil.

Because we used three different oil impregnation techniques on a wide range of grain sizes, our oil impregnation will result in different thicknesses of oil. We can envisage two possible extreme states, with the first being a conformal coating of individual grains, leaving gaps between the coated grains, and the second being a thick layer completely coating grains and filling the pores between them. However, there is also an intermediate state, with the possibility of a conformal coating of grains, but a partial filling of the pores between the grains. To investigate these possibilities, we performed LSFCM analysis on median grain sizes of 15 μm (phi 6.47), 77 μm (phi 3.73), 231 μm (phi 2.12) and 533 μm (phi 0.99), using the three oil impregnation techniques. We measured the average thickness of the oil between the grains on nine single points on all 12 oil-impregnated hydrophobic model soils.

Figure 5 shows the results of these measurements. For grain size 15 μm (phi 6.47), the measured oil thicknesses were 0.85 μm, 1.3 μm and 3.1 μm, which are all substantially smaller than the grain size itself. The thick and thin oil coating scenarios show an increase in oil

thickness with increasing grain size, approaching around 40% of the grain size. The thinnest oil coating reaches a maximum thickness of ~64 μm between 231 μm (phi 2.12) and 533 μm (phi 0.99) median grain sizes, representing 15–30% of the grain size. Figure 6a–c illustrates these changes for the 77 μm (phi 3.73) median grain size. This corresponds to Figure 4b, which shows an increase in sliding angle from 1.5° to 10.25° as the oil coating thickness decreases. The red haze from the Nile red dye shows that in all cases the grains have a thin coating of oil across the entirety of their upper surface. This is consistent with the relatively low sliding angles recorded in all three cases. Figure 6d–f shows equivalent images for median grain sizes of 15 μm (phi 6.47), 231 μm (phi 2.12) and 533 μm (phi 0.99), for the thinnest (conformal) coating of oil. The naturally rough/structured form of the surface (before the oil coating) is maintained, but each grain has a conformal coating of oil. Comparisons to Figure 4b show that the sliding angle remains below 10° up to the largest median grain size of 533 μm (phi 0.99), for which the sliding angle increases to 14.4°.

5 | DISCUSSION

5.1 | Superhydrophobic soils

Our results show that before oil contamination soils composed of clay aggregates can exhibit superhydrophobicity, characterized by an apparent contact angle above 150° (Figure 3a). This supports the earlier works of McHale, Shirtcliffe, Newton, and Pyatt (2007), who showed that a

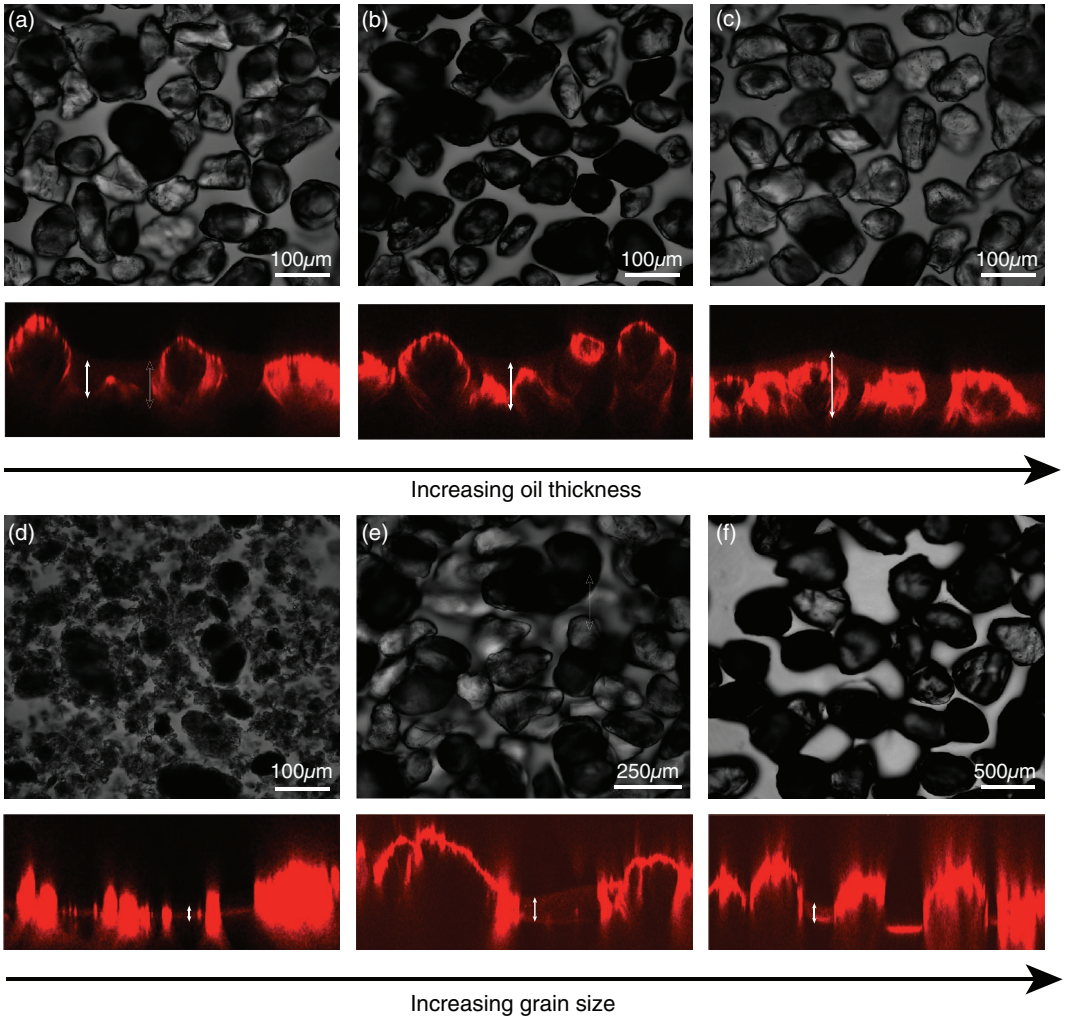

FIGURE 6 Oil impregnated samples imaged on the laser scanning fluorescence confocal microscope from top-down (black and white image) and side profiles (black and red image). In the side profiles the bright red outline shows the shape of the individual grains, with the red haze showing the oil coating. White arrows indicate the thickness of the oil. Panels (a) to (c) show median grain size 77 μm (phi 3.73) soils impregnated with (a) a thick oil coating (b) a thin oil coating and (c) a conformal oil coating. The lower panels show a conformal oil coating on median grain size (d) 15 μm (6.47), (e) 231 μm (2.12) and (f) 533 μm (0.99) [Color figure can be viewed at wileyonlinelibrary.com]

Cassie-Baxter wetting regime could exist in water-repellent soils, and where this is extreme, has the potential to create superhydrophobicity. For soils where studies have used either real soils consisting of a mixture of different grain sizes (Bachmann et al., 2006; Leelamanie, Karube, & Yoshida, 2008) or where grain fractions as small as clay or clay aggregates were not isolated in grain size-dependent contact angle studies (Saulick, Lourenço, and Baudet (2016), typical values of contact angles are reported in the range of 100–130°. Higher contact angles have been recorded in model soils; for example, Bachmann et al. (2013) measured contact angles of 140° using a small-scale contact angle measurement technique, and Ng and Lourenço (2016) report angles up to 143° for silane-treated soils. Contact angles of ≥150° have also been observed on structured surfaces composed of silica particles up to 10 μm (e.g., Cao, Jones, Sikka, Wu, & Gao, 2009; Tsai, Yang, & Lee, 2006) and on particle assembled surfaces where particle sizes range from the nanometric to hundreds of microns (e.g. McHale et al., 2005; Roach et al., 2008). We therefore consider the high contact angle values recorded in this study, particularly for the smaller grain sizes, as arising from the topography of the sieved grains and their attachment to the substrate providing a high aspect ratio, which amplified the intrinsic hydrophobicity of the surface chemistry.

We also observed a shift in wetting regime on the hydrophobic surfaces, with apparent contact angles decreasing and CAH increasing with increasing grain size (Figure 3a), illustrating the shift between a "slippy" Cassie-Baxter and "sticky" Wenzel state. At lower grain sizes the droplet sits in a Cassie-Baxter state, with high droplet mobility because of the increase in the fraction of the water–air interface below the droplet. For larger grain sizes, the droplet begins to penetrate the surface structure, resulting in lower droplet mobility, due to more solid surface contact. This is consistent with observations of other soils (de Jonge et al., 1999; Doerr et al., 1996; Saulick et al., 2016) and synthetically created textured hydrophobic surfaces (Erbil et al., 2003; McHale et al., 2005; Öner & McCarthy, 2000; Yeh, Chen, & Chang, 2008).

Although we rule out an effect of the mineralogy on the hydrophobicity of the grains due to the homogeneous surface chemistry created by the siloxane-based hydrophobizing agent, because the topography of natural surfaces such as soils and sediments, which are much more complex and heterogeneous than the synthetic surfaces created in material physics, it is more likely that the droplet will be in neither a pure Cassie-Baxter nor a pure Wenzel state (Shirtcliffe, McHale, Atherton, & Newton, 2010). This is illustrated by the plateau in sliding angle between 58 and 275 μm (phi 4.47–1.87) in Figure 3b, which we believe is caused by the droplet being in a partially penetrating wetting regime (Chang, Hong, Sheng, & Tsao, 2009).

5.2 | Soils-based SLIPS

Silicone oil can be expected to completely wet hydrophobic grains and will preferentially wet them compared to water (McHale et al., 2019; Smith et al., 2013). Therefore, we expect that droplets of water will always rest on the oil on our oil-impregnated hydrophobic model soils and would not displace the oil layer. This also prevents the water droplet from interacting with the underlying grains to an extent dependent on the oil thickness, as illustrated by the varying sliding angles on the three oil thickness scenarios (Figure 4b). With this, we were able to create soils-based SLIPS with all three thicknesses of oil characterized by sliding angles of less than 5°, up to a median grain size of 231 μm (phi 2.12). Despite the most efficient water-shedding properties being observed on the thick and thin coatings of oil, sliding angles on the thinnest layer of oil are also extremely low in comparison to the hydrophobic soil. This extreme water-shedding ability on thin conformal oil layers is highlighted by the creation of SLIPS on median grain sizes up to 32 μm (phi 5.50). Therefore, we conclude the significant improvement in water-shedding ability of the hydrophobic oil-impregnated soils seen in Figure 4b compared to that observed for the hydrophobic soils in Figure 3b, arises from the thin coating of oil on the grains stabilized by capillary forces from the surface hydrophobic chemistry. Until now, this phenomenon has only been observed in human-made materials and biological surfaces (Wong et al., 2011). Figure 4b further shows that increasing grain size results in an increase in sliding angle and we can therefore assume more force is required to move the droplet across the surface. Roughness and porosity are important factors for creating SLIPS; where the pores are sufficiently small, the lubricant (in this case silicone oil) can bridge the pores between the grains and provide a smooth slippery surface, whereby water droplets cannot penetrate the structure (Niemelä-Anttonen et al., 2018). The increase in sliding angle with increasing grain size suggests that the oil is not thick enough to smooth the macroscale roughness of the model soils, leading to partial penetration of the droplet to the structure (Tonelli, Peppou-Chapman, Ridi, & Neto, 2019). This is further supported by the LSFCM analysis (Figure 5 and Figure 6), which shows that oil thickness on the largest grain size does not exceed 40% of the grain size even for the thick layer of oil scenario.

Current research on SLIPS focuses on their use in material science and engineering by harnessing their

water-shedding and icephobic properties for purposes such as anti-icing in aviation (Tas, Memon, Xu, Ahmed, & Hou, 2020), anti-wetting in biomedical devices (Wong et al., 2011) and anti-biofouling in marine engineering (Keller et al., 2019; Xiao et al., 2013). These impacts, however, have not yet been investigated in an environment where SLIPS could occur in soils or sediment and prevent water infiltration to a greater extent than hydrophobicity. The extreme water-shedding abilities of SLIPS are achieved without the need for high contact angles whilst also resisting adhesion of other substances such as ice and microbes. The impact of these properties will have important implications for soil science and wider earth processes. For example, due to the stability of the thin oil layers, it is unlikely that repeated wetting cycles will remediate the water repellence and water-shedding properties, as is sometimes seen in other hydrophobic soils (Quyum, Achari, & Goodman, 2002). Furthermore, the stability of these surfaces, demonstrated by the creation of very thin conformal oil layers that are not removed by gravity or an immiscible liquid, highlights how little oil contamination is needed for these extreme water-shedding properties to exist. This provides a possible mechanism for long-lasting water repellence in areas of oil contamination, such as that seen at old oil spill sites in Alberta, Canada (Roy et al., 1999; Roy & McGill, 2000). Furthermore, our study shows that soil SLIPS could have important water-shedding properties with micron-thick oil coatings, which might go undetected in field studies. Such properties have the potential to impact other soil and sediment processes, such as debris flow events, to which hydrophobic soils and sediments are susceptible, and potentially, wider sediment transport processes such as sediment fan formation.

6 | CONCLUSION

By creating a thermodynamically stable oil layer on model hydrophobic soils, we show a potential mechanism for a surface to acquire water-shedding properties. On these surfaces, the apparent contact angle does not need to take on the extreme values that must occur on extreme water-repellent oil-free soils to have effective water-shedding properties. Such oil coatings can occur through human activity (e.g., oil spills) or natural processes (e.g., hydrocarbon seepage from sedimentary basins). Because the oil preferentially wets the hydrophobic soil and is maintained by capillary forces, depletion of excess oil by water erosion may not remove even the thinnest coating of oil and may therefore maintain its water-shedding properties. It is also the case that oil-coated grains may combine with a larger-scale roughness/structure to create Cassie-Baxter states (water droplets are suspended on the structure) and Wenzel states (water droplets penetrate the structure) (McHale et al., 2019). These results have important implications for our understanding of soil mechanics where a soil may become contaminated with an oil. We also believe the processes reported here, inspired by *Nepenthes* pitcher plants and their synthetic material analogues (SLIPS/LIS), may provide new mechanisms for hydrophobic and water-shedding properties in shallow slope earth systems, including soil environments and other sedimentary and slope processes, such as debris flows and sediment fan formation.

ACKNOWLEDGEMENTS

We would like to acknowledge Dr G.G. Wells and Dr P. Agrawal for their advice, technical support and guidance. We also thank the two anonymous reviewers who provided helpful comments. R. McCerery would like to acknowledge Northumbria University at Newcastle for financial support.

CONFLICT OF INTEREST

No conflict of interest to declare.

DATA AVAILABILITY STATEMENT

Data available in the Supplementary Material.

ORCID

Rebecca McCerery https://orcid.org/0000-0001-6520-3667

REFERENCES

Atherton, S., Polak, D., Hamlett, C. A. E., Shirtcliffe, N. J., McHale, G., Ahn, S., ... Newton, M. I. (2016). Drop impact behaviour on alternately hydrophobic and hydrophilic layered bead packs. *Chemical Engineering Research and Design*, *110*, 200–208.

Aussillous, P., & Quéré, D. (2001). Liquid marbles. *Nature*, *411*, 924–927. https://doi.org/10.1038/35082026

Bachmann, J., Arye, G., Deurer, M., Woche, S. K., Horton, R., Hartge, K.-H., & Chen, Y. (2006). Universality of a surface tension—Contact-angle relation for hydrophobic soils of different texture. *Journal of Plant Nutrition and Soil Science*, *169*, 745–753. https://doi.org/10.1002/jpln.200622022

Bachmann, J., Ellies, A., & Hartge, K. H. (2000). Development and application of a new sessile drop contact angle method to assess soil water repellency. *Journal of Hydrology*, *231*, 66–75.

Bachmann, J., Goebel, M.-O., & Woche, S. K. (2013). Small-scale contact angle mapping on undisturbed soil surfaces. *Journal of Hydrology and Hydromechanics*, *61*, 3–8.

Bachmann, J., Guggenberger, G., Baumgartl, T., Ellerbrock, R. H., Urbanek, E., Goebel, M.-O., ... Fischer, W. R. (2008). Physical carbon-sequestration mechanisms under special consideration

of soil wettability. *Journal of Plant Nutrition and Soil Science*, *171*, 14–26. https://doi.org/10.1002/jpln.200700054

Bachmann, J., Horton, R., van der Ploeg, R. R., & Woche, S. (2000). Modified sessile drop method for assessing initial soil–water contact angle of sandy soil. *Soil Science Society of America Journal*, *64*, 564–567. https://doi.org/10.2136/sssaj2000.642564x

Barthlott, W., & Neinhuis, C. (1997). Purity of the sacred lotus, or escape from contamination in biological surfaces. *Planta*, *202*, 1–8. https://doi.org/10.1007/s004250050096

Bauer, U., & Federle, W. (2009). The insect-trapping rim of Nepenthes pitchers. *Plant Signaling & Behavior*, *4*, 1019–1023. https://doi.org/10.4161/psb.4.11.9664

Blackwell, P. (2000). Management of water repellency in Australia, and risks associated with preferential flow, pesticide concentration and leaching. *Journal of Hydrology*, *231–232*, 384–395. https://doi.org/10.1016/S0022-1694(00)00210-9

Cannon, S. H., Bigio, E. R., & Mine, E. (2001). A process for fire-related debris flow initiation, Cerro Grande fire, New Mexico. *Hydrological Processes*, *15*, 3011–3023. https://doi.org/10.1002/hyp.388

Cannon, S. H., Gartner, J. E., Wilson, R. C., Bowers, J. C., & Laber, J. L. (2008). Storm rainfall conditions for floods and debris flows from recently burned areas in southwestern Colorado and southern California. *Geomorphology*, *96*, 250–269. https://doi.org/10.1016/j.geomorph.2007.03.019

Canny, J. (1986). A computational approach to edge detection. *IEEE Transactions on Pattern Analysis and Machine Intelligence*, *PAMI, 8*, 679–698.

Cao, L., Jones, A. K., Sikka, V. K., Wu, J., & Gao, D. (2009). Anti-icing superhydrophobic coatings. *Langmuir*, *25*, 12444–12448. https://doi.org/10.1021/la902882b

Cassie, A. B. D., & Baxter, S. (1944). Wettability of porous surfaces. *Transactions of the Faraday Society*, *40*, 546. https://doi.org/10.1039/tf9444000546

Chang, F.-M., Hong, S.-J., Sheng, Y.-J., & Tsao, H.-K. (2009). High contact angle hysteresis of superhydrophobic surfaces: Hydrophobic defects. *Applied Physics Letters*, *95*, 064102. https://doi.org/10.1063/1.3204006

Chau, H. W., Goh, Y. K., Vujanovic, V., & Si, B. C. (2012). Wetting properties of fungi mycelium alter soil infiltration and soil water repellency in a γ-sterilized wettable and repellent soil. *Fungal Biology*, *116*, 1212–1218. https://doi.org/10.1016/j.funbio.2012.10.004

Cui, J., Zhu, H., Tu, Z., Niu, D., Liu, G., Bei, Y., & Zhu, Q. (2019). Effect of the texture geometry on the slippery behavior of liquid-infused nanoporous surfaces. *Journal of Materials Science*, *54*, 2729–2739. https://doi.org/10.1007/s10853-018-2972-2

Dai, X., Stogin, B. B., Yang, S., & Wong, T.-S. (2015). Slippery wenzel state. *ACS Nano*, *9*, 9260–9267. https://doi.org/10.1021/acsnano.5b04151

de Jonge, L. W., Jacobsen, O. H., & Moldrup, P. (1999). Soil water repellency: Effects of water content, temperature, and particle size. *Soil Science Society of America Journal*, *63*, 437–442. https://doi.org/10.2136/sssaj1999.03615995006300030003x

de Jonge, L. W., Moldrup, P., & Jacobsen, O. H. (2007). Soil-water content dependency of water repellency in soils: Effect of crop type, soil management, and physical-chemical parameters. *Soil Science*, *172*, 577–588. https://doi.org/10.1097/Ss.06013e318065c090

DeBano, L. F. (2000). The role of fire and soil heating on water repellency in wildland environments: A review. *Journal of Hydrology*, *231–232*, 195–206. https://doi.org/10.1016/S0022-1694(00)00194-3

Dekker, L. W., Doerr, S. H., Oostindie, K., Ziogas, A. K., & Ritsema, C. J. (2001). Water repellency and critical soil water content in a dune sand. *Soil Science Society of America Journal*, *65*, 1667–1674. https://doi.org/10.2136/sssaj2001.1667

Dekker, L. W., & Ritsema, C. J. (1994). How water moves in a water repellent sandy soil: 1. Potential and actual water repellency. *Water Resources Research*, *30*, 2507–2517. https://doi.org/10.1029/94WR00749

DiBiase, R. A., & Lamb, M. P. (2020). Dry sediment loading of headwater channels fuels post-wildfire debris flows in bedrock landscapes. *Geology*, *48*, 189–193. https://doi.org/10.1130/G46847.1

Doerr, S. H., Dekker, L. W., Ritsema, C. J., Shakesby, R. A., & Bryant, R. (2002). Water repellency of soils. *Soil Science Society of America Journal*, *66*, 401–405. https://doi.org/10.2136/sssaj2002.4010

Doerr, S. H., Ritsema, C. J., Dekker, L. W., Scott, D. F., & Carter, D. (2007). Water repellence of soils: New insights and emerging research needs. *Hydrological Processes*, *21*, 2223–2228. https://doi.org/10.1002/hyp.6762

Doerr, S. H., Shakesby, R. A., Blake, W. H., Chafer, C. J., Humphreys, G. S., & Wallbrink, P. J. (2006). Effects of differing wildfire severities on soil wettability and implications for hydrological response. *Journal of Hydrology*, *319*, 295–311. https://doi.org/10.1016/j.jhydrol.2005.06.038

Doerr, S. H., Shakesby, R. A., & Walsh, R. P. D. (1996). Soil hydrophobicity variations with depth and particle size fraction in burned and unburned Eucalyptus globulus and *Pinus pinaster* forest terrain in the Águeda Basin, Portugal. *Catena*, *27*, 25–47. https://doi.org/10.1016/0341-8162(96)00007-0

Doerr, S. H., Shakesby, R. A., & Walsh, R. P. D. (1998). Spatial variability of soil hydrophobicity in fire-prone eucalyptus and pine forests, Portugal. *Soil Science*, *163*, 313–324. https://doi.org/10.1097/00010694-199804000-00006

Doerr, S. H., Shakesby, R. A., & Walsh, R. P. D. (2000). Soil water repellency: Its causes, characteristics and hydro-geomorphological significance. *Earth-Science Reviews*, *51*, 33–65. https://doi.org/10.1016/S0012-8252(00)00011-8

Ellis, R., & Adams, R. S. (1961). Contamination of soils by petroleum hydrocarbons. In A. G. Norman (Ed), *Advances in agronomy* (pp. 197–216). Cambridge, Massachusetts: Academic Press.

Erbil, H., Demirel, A. L., Avci, Y., & Mert, O. (2003). Transformation of a simple plastic into a superhydrophobic surface. *Science*, *299*, 1377–1380. https://doi.org/10.1126/science.1078365

Fitzgibbon, A., Pilu, M., & Fisher, R. B. (1999). Direct least square fitting of ellipses. *IEEE Transactions on pattern analysis and machine intelligence*, *21*(5), 476–480.

Geraldi, N. R., Guan, J. H., Dodd, L. E., Maiello, P., Xu, B. B., Wood, D., … McHale, G. (2019). Double-sided slippery liquid-infused porous materials using conformable mesh. *Scientific Reports*, *9*, 13280. https://doi.org/10.1038/s41598-019-49887-3

Guan, J. H., Wells, G. G., Xu, B., McHale, G., Wood, D., Martin, J., & Stuart-Cole, S. (2015). Evaporation of sessile droplets on slippery liquid-infused porous surfaces (SLIPS). *Langmuir*, *31*, 11781–11789. https://doi.org/10.1021/acs.langmuir.5b03240

Hallett, P.D. 2007. An introduction to soil water repellency. In R.E. Gaskin (Ed.), *Proceedings of the 8th International Symposium on Adjuvants for Agrochemicals* (pp. 6–9). Columbus, OH: International Society for Agrochemical Adjuvants.

Hallett, P. D., Baumgartl, T., & Young, I. M. (2001). Subcritical water repellency of aggregates from a range of soil management practices. *Soil Science Society of America Journal*, *65*, 184–190. https://doi.org/10.2136/sssaj2001.651184x

Hamlett, C. A. E., Atherton, S., Shirtcliffe, N. J., McHale, G., Ahn, S., Doerr, S. H., ... Newton, M. I. (2013). Transitions of water-drop impact behaviour on hydrophobic and hydrophilic particles. *European Journal of Soil Science*, *64*, 324–333. https://doi.org/10.1111/ejss.12003

Hamlett, C. A. E., Shirtcliffe, N. J., McHale, G., Ahn, S., Bryant, R., Doerr, S. H., & Newton, M. I. (2011). Effect of particle size on droplet infiltration into hydrophobic porous media as a model of water repellent soil. *Environmental Science & Technology*, *45*, 9666–9670. https://doi.org/10.1021/es202319a

Ibekwe, A., Tanino, Y., & Pokrajac, D. (2019). A low-cost, non-hazardous protocol for surface texturing of glass particles. *Tribology Letters*, *67*, 115. https://doi.org/10.1007/s11249-019-1230-3

Jordán, A., Zavala, L. M., Mataix-Solera, J., & Doerr, S. H. (2013). Soil water repellency: Origin, assessment and geomorphological consequences. *Catena*, *108*, 1–5. https://doi.org/10.1016/j.catena.2013.05.005

Keller, N., Bruchmann, J., Sollich, T., Richter, C., Thelen, R., Kotz, F., ... Rapp, B. E. (2019). Study of biofilm growth on slippery liquid-infused porous surfaces made from fluoropor. *ACS Applied Materials & Interfaces*, *11*, 4480–4487. https://doi.org/10.1021/acsami.8b12542

Lafuma, A., & Quéré, D. (2011). Slippery pre-suffused surfaces. *EPL (Europhysics Letters)*, *96*, 56001. https://doi.org/10.1209/0295-5075/96/56001

Landau, L., & Levich, B. (1988). Dragging of a liquid by a moving plate. In P. Pelce & A. Libchaber (Eds), *Dynamics of curved fronts* (pp. 141–153). San Diego: Academic Press.

Launay, G. (2018). PyDSA_core: drop shape analysis in python. https://framagit.org/gabylaunay/pyDSA_core. [Online; accessed: 12th Nov 2019].

Leelamanie, D. A. L., & Karube, J. (2007). Effects of organic compounds, water content and clay on the water repellency of a model sandy soil. *Soil Science and Plant Nutrition*, *53*, 711–719. https://doi.org/10.1111/j.1747-0765.2007.00199.x

Leelamanie, D. A. L., & Karube, J. (2012). Drop size dependence of soil-water contact angle in relation to the droplet geometry and line tension. *Soil Science and Plant Nutrition*, *58*, 675–683. https://doi.org/10.1080/00380768.2012.745798

Leelamanie, D. A. L., Karube, J., & Yoshida, A. (2008). Characterizing water repellency indices: Contact angle and water drop penetration time of hydrophobized sand. *Soil Science and Plant Nutrition*, *54*, 179–187. https://doi.org/10.1111/j.1747-0765.2007.00232.x

Letey, J., Osborn, J., & Pelishek, R. E. (1962). The influence of the water-solid contact angle on water movement in soil. *Hydrological Sciences Journal*, *7*, 75–81. https://doi.org/10.1080/02626666209493272

Linder, M. B. (2009). Hydrophobins: Proteins that self assemble at interfaces. *Current Opinion in Colloid & Interface Science*, *14*, 356–363. https://doi.org/10.1016/j.cocis.2009.04.001

Maimon, A., Gross, A., & Arye, G. (2017). Greywater-induced soil hydrophobicity. *Chemosphere*, *184*, 1012–1019. https://doi.org/10.1016/j.chemosphere.2017.06.080

Mataix-Solera, J., García-Irles, L., Morugán, A., Doerr, S. H., Garcia-Orenes, F., Arcenegui, V., & Atanassova, I. (2011). Longevity of soil water repellency in a former wastewater disposal tree stand and potential amelioration. *Geoderma*, *165*, 78–83. https://doi.org/10.1016/j.geoderma.2011.07.006

McHale, G., Newton, M. I., & Shirtcliffe, N. J. (2005). Water-repellent soil and its relationship to granularity, surface roughness and hydrophobicity: A materials science view. *European Journal of Soil Science*, *56*, 445–452. https://doi.org/10.1111/j.1365-2389.2004.00683.x

McHale, G., Orme, B. V., Wells, G. G., & Ledesma-Aguilar, R. A. (2019). Apparent contact angles on lubricant impregnated surfaces/SLIPS: From superhydrophobicity to electrowetting. *Langmuir*, *35*, 4197–4204. https://doi.org/10.1021/acs.langmuir.8b04136

McHale, G., Shirtcliffe, N. J., Newton, M. I., & Pyatt, F. B. (2007). Implications of ideas on super-hydrophobicity for water repellent soil. *Hydrological Processes*, *21*, 2229–2238. https://doi.org/10.1002/hyp.6765

McHale, G., Shirtcliffe, N. J., Newton, M. I., Pyatt, F. B., & Doerr, S. H. (2007). Self-organization of hydrophobic soil and granular surfaces. *Applied Physics Letters*, *90*, 054110. https://doi.org/10.1063/1.2435594

Neinhuis, C. (1997). Characterization and distribution of water-repellent, self-cleaning plant surfaces. *Annals of Botany*, *79*, 667–677. https://doi.org/10.1006/anbo.1997.0400

Ng, S. H. Y., & Lourenço, S. D. N. (2016). Conditions to induce water repellency in soils with dimethyldichlorosilane. *Geotechnique*, *66*, 441–444. https://doi.org/10.1680/jgeot.15.T.025

Niemelä-Anttonen, H., Koivuluoto, H., Tuominen, M., Teisala, H., Juuti, P., Haapanen, J., ... Vuoristo, P. (2018). Icephobicity of slippery liquid infused porous surfaces under multiple freeze-thaw and ice accretion-detachment cycles. *Advanced Materials Interfaces*, *5*, 1800828. https://doi.org/10.1002/admi.201800828

Nosonovsky, M. (2011). Slippery when wetted. *Nature*, *477*, 412–413. https://doi.org/10.1038/477412a

Öner, D., & McCarthy, T. J. (2000). Ultrahydrophobic surfaces. Effects of topography length scales on wettability. *Langmuir*, *16*, 7777–7782. https://doi.org/10.1021/la000598o

Parise, M., & Cannon, S. H. (2012). Wildfire impacts on the processes that generate debris flows in burned watersheds. *Natural Hazards*, *61*, 217–227. https://doi.org/10.1007/s11069-011-9769-9

Piccolo, A., Spaccini, R., Haberhauer, G., & Gerzabek, M. H. (1999). Increased sequestration of organic carbon in soil by hydrophobic protection. *Naturwissenschaften*, *86*, 496–499. https://doi.org/10.1007/s001140050662

Quére, D., Lafuma, A., & Bico, J. (2003). Slippy and sticky microtextured solids. *Nanotechnology*, *14*, 1109–1112. https://doi.org/10.1088/0957-4484/14/10/307

Quyum, A., Achari, G., & Goodman, R. H. (2002). Effect of wetting and drying and dilution on moisture migration through oil contaminated hydrophobic soils. *Science of the Total Environment*, *296*, 77–87. https://doi.org/10.1016/S0048-9697(02)00046-3

Regalado, C. M., & Ritter, A. (2006). Geostatistical tools for characterizing the spatial variability of soil water repellency

parameters in a Laurel forest watershed. *Soil Science Society of America Journal*, *70*, 1071–1081. https://doi.org/10.2136/sssaj2005.0177

Roach, P., Shirtcliffe, N. J., & Newton, M. I. (2008). Progess in superhydrophobic surface development. *Soft Matter*, *4*, 224–240. https://doi.org/10.1039/B712575P

Robichaud, P. R., Lewis, S. A., & Ashmun, L. E. (2008). *New procedure for sampling infiltration to assess post-fire soil water repellency* (Res. Note. RMRS-RN-33). Fort Collins, CO: U.S. Department of Agriculture, Forest Service, Rocky Mountain Research Station.

Roy, J. L., & McGill, W. B. (1998). Characterization of disaggregated nonwettable surface soils found at old crude oil spill sites. *Canadian Journal of Soil Science*, *78*, 331–344. https://doi.org/10.4141/S97-039

Roy, J. L., & McGill, W. B. (2000). Investigation into mechanisms leading to the development, spread and persistence of soil water repellency following contamination by crude oil. *Canadian Journal of Soil Science*, *80*, 595–606. https://doi.org/10.4141/S99-091

Roy, J. L., & McGill, W. B. (2002). Assessing soil water repellency using the molarity of ethanol droplet (MED) test. *Soil Science*, *167*, 83–97. https://doi.org/10.1097/00010694-200202000-00001

Roy, J. L., McGill, W. B., & Rawluk, M. D. (1999). Petroleum residues as water-repellent substances in weathered nonwettable oil-contaminated soils. *Canadian Journal of Soil Science*, *79*, 367–380. https://doi.org/10.4141/S97-040

Saulick, Y., Lourenço, S. & Baudet, B. 2016. Effect of particle size on the measurement of the apparent contact angle in sand of varying wettability under air-dried conditions. P. Delage, Y.-J. Cui, S. Ghabezloo, J.-M. Pereira and A.-M. Tang In E3S Web of Conferences, Vol. 9.

Schaumann, G. E., Braun, B., Kirchner, D., Rotard, W., Szewzyk, U., & Grohmann, E. (2007). Influence of biofilms on the water repellency of urban soil samples. *Hydrological Processes*, *21*, 2276–2284. https://doi.org/10.1002/hyp.6746

Seiwert, J., Clanet, C., & Quéré, D. (2011). Coating of a textured solid. *Journal of Fluid Mechanics*, *669*, 55–63.

Semprebon, C., Mchale, G., & Kusumaatmaja, H. (2017). Apparent contact angle and contact angle hysteresis on liquid infused surfaces. *Soft Matter*, *13*, 101–110.

Shakesby, R. A., Doerr, S. H., & Walsh, R. P. D. (2000). The erosional impact of soil hydrophobicity: Current problems and future research directions. *Journal of Hydrology*, *231–232*, 178–191. https://doi.org/10.1016/S0022-1694(00)00193-1

Shirtcliffe, N. J., Aqil, S., Evans, C., McHale, G., Newton, M. I., Perry, C. C., & Roach, P. (2004). The use of high aspect ratio photoresist (SU-8) for super-hydrophobic pattern prototyping. *Journal of Micromechanics and Microengineering*, *14*, 1384–1389. https://doi.org/10.1088/0960-1317/14/10/013

Shirtcliffe, N. J., McHale, G., Atherton, S., & Newton, M. I. (2010). An introduction to superhydrophobicity. *Advances in Colloid and Interface Science*, *161*, 124–138. https://doi.org/10.1016/j.cis.2009.11.001

Smith, J. D., Dhiman, R., Anand, S., Reza-Garduno, E., Cohen, R. E., McKinley, G. H., & Varanasi, K. K. (2013). Droplet mobility on lubricant-impregnated surfaces. *Soft Matter*, *9*, 1772–1780. https://doi.org/10.1039/C2SM27032C

Spaccini, R., Piccolo, A., Conte, P., Haberhauer, G., & Gerzabek, M. H. (2002). Increased soil organic carbon sequestration through hydrophobic protection by humic substances. *Soil Biology and Biochemistry*, *34*, 1839–1851. https://doi.org/10.1016/S0038-0717(02)00197-9

Tao, R., Mchale, G., Reboud, J., Cooper, J. M., Torun, H., Luo, J. T., … Fu, Y. (2020). Hierarchical nanotexturing enables acoustofluidics on slippery yet sticky, flexible surfaces. *Nano Letters*, *20*, 3263–3270. https://doi.org/10.1021/acs.nanolett.0c00005

Tas, M., Memon, H., Xu, F., Ahmed, I., & Hou, X. (2020). Electrospun nanofibre membrane based transparent slippery liquid-infused porous surfaces with icephobic properties. *Colloids and Surfaces A: Physicochemical and Engineering Aspects*, *585*, 124177. https://doi.org/10.1016/j.colsurfa.2019.124177

Tessler, N., Wittenberg, L., Malkinson, D., & Greenbaum, N. (2008). Fire effects and short-term changes in soil water repellency – Mt. Carmel, Israel. *Catena*, *74*, 185–191. https://doi.org/10.1016/j.catena.2008.03.002

Tonelli, M., Peppou-Chapman, S., Ridi, F., & Neto, C. (2019). Effect of pore size, lubricant viscosity, and distribution on the slippery properties of infused cement surfaces. *Journal of Physical Chemistry C*, *123*, 2987–2995.

Tsai, P. S., Yang, Y. M., & Lee, Y. L. (2006). Fabrication of hydrophobic surfaces by coupling of Langmuir-Blodgett deposition and a self-assembled monolayer. *Langmuir*, *22*, 5660–5665. https://doi.org/10.1021/la053152m

Utermann, S., Aurin, P., Benderoth, M., Fischer, C., & Schröter, M. (2011). Tailoring the frictional properties of granular media. *Physical Review E*, *84*, 031306. https://doi.org/10.1103/PhysRevE.84.031306

Van Dam, J. C., Hendrickx, J. M. H., Van Ommen, H. C., Bannink, M. H., Van Genuchten, M. T., & Dekker, L. W. (1990). Water and solute movement in a coarse-textured water-repellent field soil. *Journal of Hydrology*, *120*, 359–379. https://doi.org/10.1016/0022-1694(90)90159-U

van Ommen, H. C., Dekker, L. W., Dijksma, R., Hulshof, J., & van der Molen, W. H. (1988). A new technique for evaluating the presence of preferential flow paths in nonstructured soils. *Soil Science Society of America Journal*, *52*, 1192–1193. https://doi.org/10.2136/sssaj1988.03615995005200040056x

Wang, P., Zhang, D., & Lu, Z. (2015). Slippery liquid-infused porous surface bio-inspired by pitcher plant for marine anti-biofouling application. *Colloids and Surfaces B: Biointerfaces*, *136*, 240–247. https://doi.org/10.1016/j.colsurfb.2015.09.019

Wang, Y., Wang, X., Chau, H. W., Si, B., Yao, N., & Li, Y. (2018). Water movement and finger flow characterization in homogeneous water-repellent soils. *Vadose Zone Journal*, *17*, 1–12. https://doi.org/10.2136/vzj2018.01.0021

Wenzel, R. N. (1936). Resistance of solid surfaces to wetting by water. *Industrial & Engineering Chemistry*, *28*, 988–994. https://doi.org/10.1021/ie50320a024

Wessels, J. G. H. (1996). Fungal hydrophobins: Proteins that function at an interface. *Trends in Plant Science*, *1*, 9–15. https://doi.org/10.1016/S1360-1385(96)80017-3

Wilson, P. W., Lu, W., Xu, H., Kim, P., Kreder, M. J., Alvarenga, J., & Aizenberg, J. (2013). Inhibition of ice nucleation by slippery liquid-infused porous surfaces (SLIPS). *Physical Chemistry Chemical Physics*, *15*, 581–585. https://doi.org/10.1039/C2CP43586A

Wong, T.-S., Kang, S. H., Tang, S. K. Y., Smythe, E. J., Hatton, B. D., Grinthal, A., & Aizenberg, J. (2011). Bioinspired self-repairing

slippery surfaces with pressure-stable omniphobicity. *Nature*, *477*, 443–447. https://doi.org/10.1038/nature10447

Woods, S. W., Birkas, A., & Ahl, R. (2007). Spatial variability of soil hydrophobicity after wildfires in Montana and Colorado. *Geomorphology*, *86*, 465–479. https://doi.org/10.1016/j.geomorph.2006.09.015

Xiao, L., Li, J., Mieszkin, S., Di Fino, A., Clare, A. S., Callow, M. E., ... Levkin, P. A. (2013). Slippery liquid-infused porous surfaces showing marine antibiofouling properties. *ACS Applied Materials and Interfaces*, *5*, 10074–10080. https://doi.org/10.1021/am402635p

Yeh, K.-Y., Chen, L.-J., & Chang, J.-Y. (2008). Contact angle hysteresis on regular pillar-like hydrophobic surfaces. *Langmuir*, *24*, 245–251. https://doi.org/10.1021/la7020337

Young, T. I. (1832). An essay on the cohesion of fluids. *Abstracts of the Papers Printed in the Philosophical Transactions of the Royal Society of London*, *1*, 171–172. https://doi.org/10.1098/rspl.1800.0095

SUPPORTING INFORMATION

Additional supporting information may be found online in the Supporting Information section at the end of this article.

How to cite this article: McCerery R, Woodward J, McHale G, Winter K, Armstrong S, Orme BV. Slippery liquid-infused porous surfaces: The effect of oil on the water repellence of hydrophobic and superhydrophobic soils. *Eur J Soil Sci*. 2020;1–16. https://doi.org/10.1111/ejss.13053